In Vivo Osseointegration of Nano-Designed Composite Coatings on Titanium Implants

Sybille Facca,[†,‡,§,#] Debrupa Lahiri,[†,#] Florence Fioretti,[‡,⊥] Nadia Messadeq,[∥] Didier Mainard,[¶] Nadia Benkirane-Jessel,[‡,¶,*] and Arvind Agarwal[†,*]

[†]Plasma Forming Lab and Nanomechanics and Nanotribology Lab, Department of Mechanical and Materials Engineering, Florida International University, Miami, Florida 33174, United States, [‡]Biomatériaux et Ingénierie tissulaire, Faculté de Médecine, Institut National de la Santé et de la Recherche Médicale (INSERM), Unité 977, 11 rue Humann, 67085 Strasbourg Cedex, France, [§]Department of Hand Surgery, Strasbourg University Hospitals, 10 Avenue Achille Baumann, 67403 Illkirch Cedex, France, [⊥]Faculté de Chirurgie Dentaire, Université de Strasbourg, Strasbourg, France, [∥]IGBMC, Illkirch, France, and [¶]Centre d'Ortopédie de Nancy, Hôpital Central, and UMR 7561, CNRS-Université Henri Poincaré Nancy I, 29 Avenue du Maréchal de Lattre de Tassigny, 54000 Nancy, France. [#]These authors contributed equally to this work.

ABSTRACT This is the first *in vivo* study of plasma-sprayed carbon nanotube (CNT)-reinforced hydroxyapatite (HA) coating on titanium implants embedded in rodents' bone. No adverse effect or cytotoxicity of CNT addition on bone tissues and cells was observed. Normal bone growth was observed around HA–CNT-coated implants. CNT addition induces higher osseointegration as compared to HA. Elastic modulus of new bone was compared with the modulus of HA-CNT/bone interface to understand the mechanical integrity of the implant.

KEYWORDS: hydroxyapatite · carbon nanotubes · osseointegration · bone induction *in vivo* · elastic modulus · titanium implants

Hydroxyapatite (HA) is used in the biomedical industry as the coating for titanium implants. HA is also used as the structural material for dental, maxillofacial, and orthopedic implants,[1,2] but HA is known to display rapid wear and failure due to poor fracture toughness.[3] Therefore, problems such as loosening of arthroplasty prostheses continue to scare surgeons. Hence, there is still a large demand for the acceleration of new bone induction around implants for improved osseointegration.

Carbon nanotube (CNT), first reported in 1991,[4] is a potential reinforcement for brittle hydroxyapatite, as it exhibits high Young's modulus[5–7] and tensile strength.[8] CNTs are being extensively researched as reinforcement for improving the fracture toughness and wear resistance of brittle ceramics, such as HA[9–12] and Al_2O_3.[13–15] Though biocompatibility of HA is in universal agreement, the same is not true for CNT. The cytotoxicity of CNT is still in debate with contradictory reports by different research groups.[16–23] However, CNTs have been found to aid in accelerated bone growth and apatite precipitation and induce bonding and reinforcement with the bone matrix.[24–27] *In vitro* studies have shown the HA–CNT composites possess improved biocompatibility with osteoblasts[9,10,28] and macrophages.[10] However, *in vivo* response of HA–CNT composite-coated titanium implants in bones has never been explored. There are few *in vivo* studies performed with bare CNTs, but they are restricted to ectopic bone induction, tibial diaphysis, or mice skull.[24,27,29,30] CNTs help in accelerated new bone growth and guided bone regeneration in the case of defect recovery.[24,27] There is only one report on *in vivo* study of the sintered HA–CNT composite, which was performed by implanting in a rat muscle tissue but not the bone.[31] After 14 days of implantation, the muscle tissues look similar to natural undamaged tissue, which indicates recovery and no cytotoxic effect.[31]

This study reports *in vivo* investigations of HA–CNT-coated Ti-6Al-4V alloy (hereafter referred as titanium) implants of different geometries which were embedded in mice and rats. The effect of CNT addition to HA on bone healing and bone induction is elucidated. The elastic modulus of the newly grown bone was measured and compared with the coating and implant to qualitatively compare strain at the interfaces. A very sharp and large difference in the elastic modulus between the implant and bone can create a large difference in strain at the interface, resulting in failure. This study encompasses all those variables (*e.g.*, *in vivo* bone implantations, HA coating, CNT reinforcement to HA, real-life titanium alloy implant, and mechanical properties of the new bone and multiple interfaces), which

* Address correspondence to agarwala@fiu.edu, nadia.jessel@medecine.u-strasbg.fr.

Received for review February 24, 2011 and accepted May 19, 2011.

Published online May 19, 2011
10.1021/nn200768c

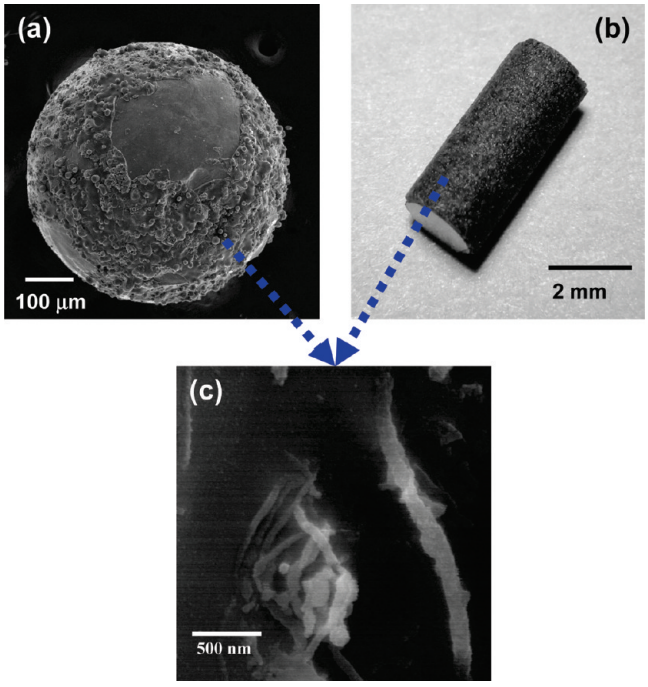

Figure 1. HA/4 wt % CNT-coated implants: (a) spherical Ti bead, (b) titanium rod, and (c) top surface of plasma-sprayed HA−CNT coating showing embedded CNTs in HA matrix. Coatings on Ti spherical bead rods were deposited using spray-dried HA and HA/4 wt % CNT powder as starting material. Plasma spraying was performed using SG 100 gun (Praxair Surface Technology, Danbury, CT) at 23 kW power. A JEOL JSM 630F scanning electron microscope (SEM) with a field emission gun was used to obtain pictures in (a) and (c). The picture of coated Ti rod was captured using a Sony DSC 400 digital camera.

are required for critical and synergistic evaluation prior to clinical translation.

RESULTS

Titanium beads or rods were implanted inside the distal part of an external condyle of the femoral bone of rodents (Figure 2a) during one month. Titanium beads and rods had three different types of coatings: (i) uncoated titanium, (ii) HA coating, and (iii) HA/4 wt % CNT coating. The coating thickness was 100−150 μm. Three groups of titanium implants were tested in the pull-out model for mice and rats: uncoated (group 1), HA coating (group 2), HA/4 wt % CNT composite coating (group 3). As a group control, a hole was made inside the femoral bone with no implant (group 4).

Clinical Results. Table 1 lists all groups including the control group. A total of 23 animals were used for this study. Each animal received only one type of implant in order to avoid systemic responses. Clinical results showed that none of the animals died during surgery or postoperatively. Rats and mice could walk without any disabilities after the implantation surgery. No infection, no disunion of the scar, and a complete range of motions of the knee joint were observed. After dissection and retrieval of all parts of the femoral bone with knee joint, no infected tissues were found (Figure 2b). X-ray images of rat femoral bones after one month of implantation from all four groups are shown in Figure 3. The implants from groups 1 (bare titanium), 2 (HA coating on titanium), and 3 (HA−CNT coating on titanium) were well-positioned inside the external femoral condyle. None of the implant was ejected. Cortical bones were restored completely, and a good healing was achieved for all four group bones after one month of implantation. We also observed good osseointegration (no osteolysis around implants) or no specific periostal reactions (sign of infection) around the three groups of implants in the rats and mice.

Histological Results. Semithin (1−2 mm) sections were cut from rat's femoral bone with the embedded implant for the microscopic observations (Figure 4a). The spherical beads in mice bones were completely removed before cutting the bone. Periostal tissue was restored for all groups, without any inflammatory reactions at the perforation location of the cortical bone. Cortical and marrow bones appeared normal around each implant (groups 1, 2, and 3) without any specific abnormal tissues. No osteolysis was observed at the periphery of the rod-shaped implants embedded inside the external femoral condyle. This also included HA−CNT composite implants (group 3), which is of greater interest for this study. For histological observations, all implants from mice and rats were fully removed from the bone using forceps. It was most difficult to detach group 3 implants (HA−CNT-coated beads and rods) as compared to groups 1 and 2, which is a qualitative indicator of the strong adherence of CNT containing HA coating with the bone.

The bone around implants of groups 1, 2, and 3 was compared with the control bones (group 4) for both

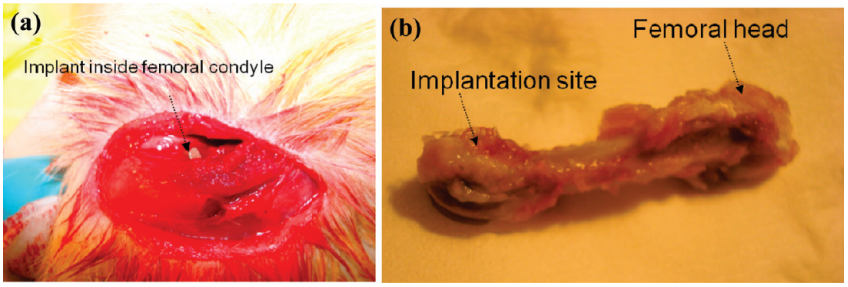

Figure 2. (a) Through a bony defect, a rod is completely introduced inside the distal rat femoral bone. (b) Rat femoral bone retrieved from group 3: HA–CNT-coated titanium implant at the distal part was recovered by periosteum. One month after implantation, mice and rats were killed with an overdose of ketamine and xylasine. For different *ex vivo* analysis, all parts of the femoral bone, from femoral head to knee joint, were excised on mice and rats and cleaned of the soft tissue. No infected or inflammatory tissues were found in groups 1, 2, 3, and 4.

TABLE 1. List of Different Types of Surgeries and Implantations on Rodents: Uncoated Titanium Implant (Group 1), HA Coating on Titanium Implant (Group 2), HA/4 wt % Coating on Titanium Implant (Group 3), and a Group Control with No Implant Just a Hole Performed (Group 4)[a]

	mice	rats
group 1 (uncoated titanium)	6 beads	2 rods
group 2 (HA coating)	4 beads	2 rods
group 3 (HA/4 wt % CNT coating)	7 beads	2 rods
group 4 (no implant)	4 holes	2 holes

[a] Holes were made in the same animal on the left femoral bone to minimize the number of sacrificial animals. Hence, a total of 17 mice and 6 rats were used for *in vivo* studies.

mice and rats. The approach was to compare *ex vivo* tissues, cell behavior, and bioactivity around implants using SEM, TEM observations, and different histological methods. Figure 4 shows the histological observations from groups 1, 2, and 3 implants embedded in mice. Bone tissues exhibited new grown bone, hematopoietic marrow, and trabecular bones, which were synthesized with osteocytes into their lacuna. Similar results were observed for the rod-shaped implants embedded in rats' bones as shown in Figure 6. After one month of surgery, the medullar cavity in group 4 was fully restored. The cortical defect for all groups was also restored due to formation of the neocortical bone. Figure 5 also shows a gray layer attached on the bone closed to the cavity (C). The layer is thicker for HA–CNT-coated implants (group 3) as compared to HA-coated (group 2) and uncoated implants (group 1). With toluidine blue coloration in Figure 7, it is clearly observed that HA–CNT coating (gray layer) was strongly attached to the newly grown bone tissues. This explains the difficulty in detaching the group 3 implants from the bone using forceps. A normal neobone near the HA–CNT coating suggests that bone regeneration was complete.

TEM Results. Transmission electron microscopy (TEM) was employed to study the bone in retrieved implants from mice and rats for all groups. Since HA–CNT coating

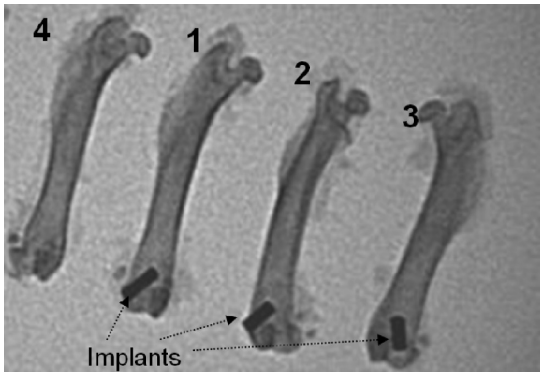

Figure 3. X-ray images of rat femoral bones after one month implantation. The distal part contains (1) uncoated titanium implant, (2) HA coating on titanium implant, (3) HA–CNT composite coating on titanium implant, and (4) no implant after the perforation of bone. The three different implants were well-positioned inside external condyle, and none of the implant was ejected. A good healing was achieved for all four bones. We observed good osseointegration (no osteolysis around implants) or no periostal reactions (sign of infection) around three bones containing implants.

is the focus of this study, TEM results from only group 3 are presented here. Other groups also displayed very similar microstructural observations from the bone (see Supporting Information, Figures S1 for TEM results from groups 1, 2, and 4). Figure 8a shows TEM images of the mice bone. Osteocytes into their lacuna with the bone matrix, osteoclasts, and osteoblasts were present. Both trabecular bone and bone marrow have been normally restored without inflammatory response. The cells inside vessels or adipocytes were also normal. No CNT was observed inside the macrophages' cytoplasm. Figure 8b shows TEM images of the rats' bones. Normal bone cells and bony trabeculum were observed without necrosis or inflammatory reaction. There was no tissue degeneration or neutrophil infiltration for HA–CNT-coated implants. CNT migration was not observed in either newly formed bone adjacent to the coating or distant bone.

Elastic Properties of the Bone/Implant Interface. Figure 4b shows the locations across the implant/bone interface,

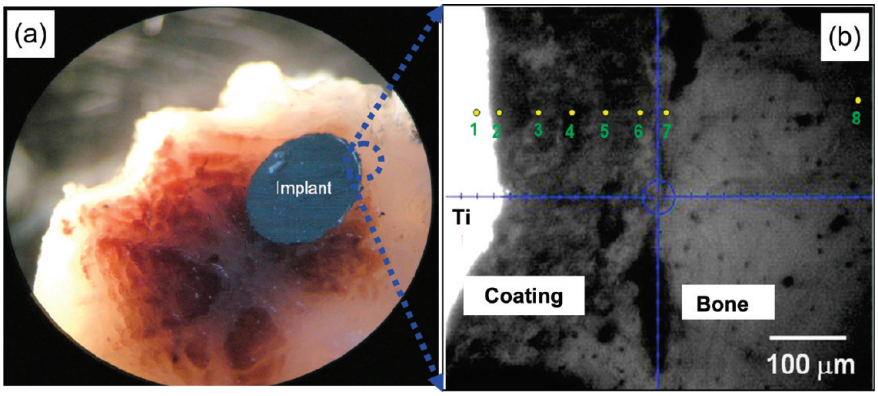

Figure 4. (a) *Ex vivo* semithin (1−2 mm) sections were cut from the rat's bone with implant embedded inside. Microscopic observations were performed at 5×. Titanium rods were fixed inside the external femoral condyle. Normal cortical bone and bone marrow were observed around the implant (group 1, 2, and 3), without any specific inflammation tissues or osteolysis. (b) Optical cross-sectional micrograph of the retrieved implant from rat showing Ti substrate, HA/HA−CNT coating, and bone. This micrograph is representative of groups 2 and 3 samples showing the locations of modulus mapping measurements by Arabic numbers. Position 1 denotes the region in the titanium part of the implant near the coating. Positions 2−6 are equally placed locations through the thickness of HA/HA−CNT coating starting from the titanium side and going toward the bone. Position 7 is in the newly grown bone along the implant surface, and position 8 is in a distant region that represents the normal bone.

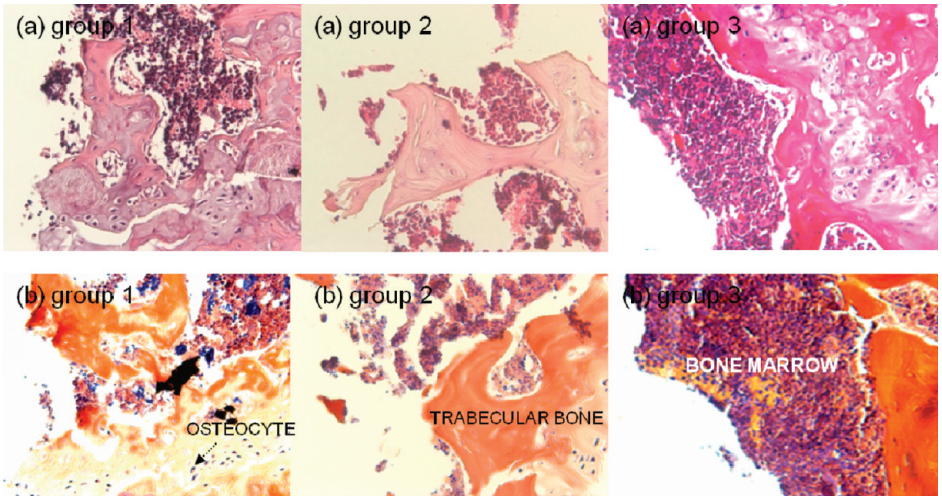

Figure 5. Histological results (40×) for mice bones which were implanted with spherical beads. (a) Mallory coloration images and (b) hematoxylin-eosine coloration images for groups 1, 2, and 3. These images show normal, thick trabecular, and hematopoietic marrow bones without any inflammatory reactions.

where modulus mapping experiments were performed on groups 2 and 3. The measurements include one region in the Ti rod near the coating, five equally spaced regions across the coating, one region in the newly generated bone near the coating, and one region far from the implant that represents the natural bone. In the case of the bare Ti implant (group 1), measurements were made in three regions *viz.* in Ti substrate, newly generated bone near Ti, and the natural bone at a distance from the implant. Modulus mapping of cross section of the bone, without any implant (group 4), was also carried out as the control sample. At least three areas of 5 μm × 5 μm were used for 2D modulus mapping from each region to obtain the representative value of the elastic modulus.

Elastic modulus of the implant/coating/bone interface is evaluated considering its significance with respect to the failure of an implant *in vivo*. Dissimilar elongation or strain in the adjacent parts at the bone/implant interface could cause localized stress generation, followed by fracture and delamination of the implant from the bone. Figure 8 is a compilation of the modulus maps for groups 1−4 implants. The color scale for the elastic modulus has been kept constant between 0 and 250 GPa for all images. It enables a clear visualization of the change in elastic modulus across the implant/coating and coating/bone interfaces. Elastic modulus for titanium was similar throughout for groups 1, 2, and 3, which indicates no change in Ti properties after *in vivo* exposure of one month, but both HA and HA−CNT coatings show changes in the elastic modulus in the retrieved implant. Elastic modulus of the coatings in groups 2 and 3 is highest near Ti and reduces gradually toward the bone, as observed from

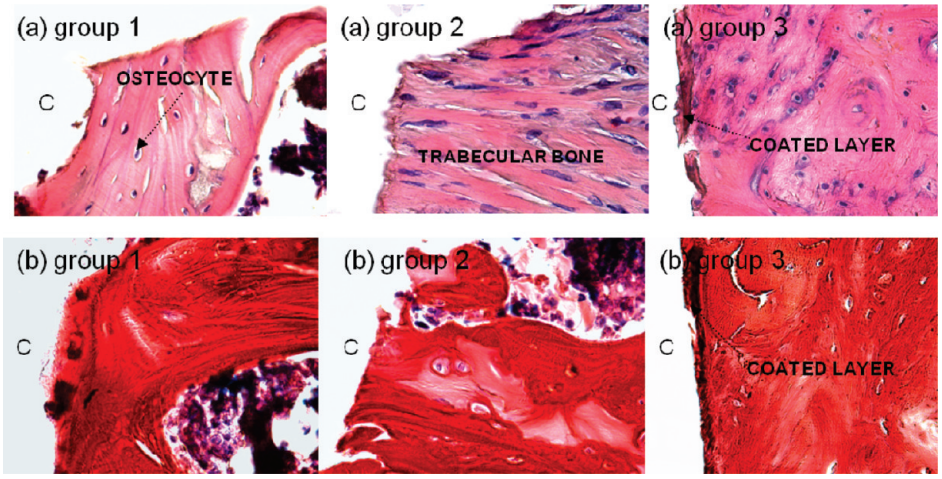

Figure 6. Histological results (40×) for rat bones with rod-shaped implants. (a) Mallory coloration images and (b) hematoxylin-eosine coloration images for groups 1, 2, and 3. These images show normal, thick trabecular, and hematopoietic marrow bones, without any inflammatory reactions and tissues. A layer is observed attached on the bone closed to the cavity (C) caused by the retrieved implant. The layer is thicker for group 3 (HA–CNT coating) and attached to newly grown bone tissues.

Figure 7. Histological image (5×) of group 3 implant in rat, with toluidine blue coloration showing HA–CNT coating strongly attached to newly grown bone tissues. Normal neobone closed to the coating with normal cell morphology was found.

the gradual change in the color of modulus maps in Figure 9. Figure 10 presents the change in an average modulus value across the distance over the implant–bone interfaces for groups 1–3 implants (see Supporting Information for methodology to obtain average elastic modulus from modulus maps). Bare Ti-implanted bone shows a very sharp change in elastic modulus across the bone–implant interface, which possess the risk of loosening of implant, fracture of bone, and delamination from the implant surface due to highest strain gradient.[32] Presence of HA–CNT and HA coatings creates a smooth gradient of elastic modulus across the implant–bone interface, which increases the mechanical compatibility of the implant with the bone and reduces the chance of fracture or implant failure. Thus, in addition to bone integration, HA-based coatings also play a vital role in maintaining the mechanical health of the implanted bone.

DISCUSSION

Clinical, histological, and TEM observations described above indicate that CNT addition promotes the formation of the new bone without any detrimental effect. Our clinical and X-ray results were the same for both rodents, with no side effects, no osteolysis, and a good osseointegration for the CNT–HA composite implants. Biocompatibility with the bone near the implant and in a distant bone was excellent. Haematopoeitic marrow and trabecula bones appeared with a good integrity; all different types of cells associated with bone suggested a normal neobone induction. The presence of osteocytes in the lacuna and the observation of bony trabecculum and osteoblats were specific for bone formation. Bioactivity and morphology of cells around all implants were completely normal. HA–CNT did not induce necrosis or inflammatory reactions[24] or formation of tissue granulomas.[18] Our promising

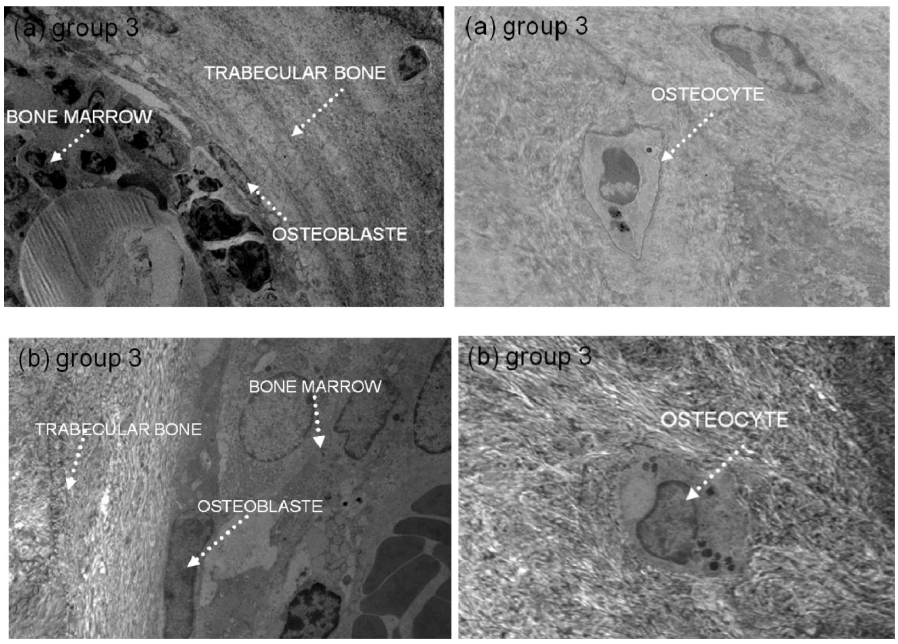

Figure 8. TEM observations of HA−CNT-coated titanium implants at 2200× magnification. Images (a) are from mice bone, whereas images (b) are from rats' bones. No abnormal cells and no CNTs were observed inside any phagocytes. In both rodents, cortical and marrow bones were perfectly restored. Osteoblast and osteocyte morphologies were normal.

results are largely attributed to the presence of CNTs that accelerate bone growth,[24] biomineralization, and inhibit osteoclastic bone resorption.[29] The accelerated bone repair occurs because CNTs stimulate osteoblast proliferation and adhesion.[33] CNTs can also form an efficient nanomatrix for the growth of HA crystals with a stoichiometric value that complies with natural HA.[25,26,34,35] Hence, CNTs act as an effective nucleation surface to induce the formation of a biomimetic apatite coating. A better adhesion was observed for HA−CNT-coated implants (group 3) which could be attributed to the nucleation of apatite on the CNT surface that promotes anchorage.[9,24,25] The higher surface area of CNTs also promotes bonding, as observed in Figure 7, where HA−CNT coating was bonded with newly grown bone. For orthopedic surgeons, osseointegration of joint replacement continues to be a challenge in terms of quality and duration, which could be improved by CNT addition to HA.

One of the controversial issues is the toxicity of CNTs on tissues[16] and cells.[36,37] Nanotoxicological potential on human macrophage cells[38,39] and phagocytes[30] could increase inflammation and decrease wound healing for orthopedic implants. It has been reported that for human macrophage cells exposed to an unpurified multiwalled carbon nanotube, a decrease in the activity was correlated with uptake of CNT due to necrosis.[38] Unpurified CNTs have been observed by transmission electronic microscopy into the cytoplasm and the nucleus. CNTs were able to enter the cell through the phenomena of endocytosis. CNTs may also cause incomplete phagocytosis *in vivo*[30] and may result in an oxidative stress and cell death *in vitro*.[38] The phenomena of phagocytosis or necrosis or any strong inflammation reactions were not observed in our study near the implant/coating/bone interface in group 3 samples with HA−CNT coating. The same observations were made for new and distant bone cells. The lack of inflammatory response is because enzymatic biodegradation of nanotubes does not induce any inflammatory response.[18] Inflammation could also be explained by the ineffective internalization of nonfunctionalized nanotubes by phagocytic cells.[40] Nanotubes are actively ingested through phagocytois in macrophages in significant quantities without cytotoxic effects.[41] It has also been shown that wear debris generated from plasma-sprayed HA−CNT coating does not alter the cytotoxicity response of macrophages.[10] Some studies even suggested that macrophages induced by nanotubes may mediate bone formation because macrophages can produce osteoinductive factors (TGF-β, BMP-2).[27]

Another novel feature of this study is the elastic modulus measurement of the new bone and its comparison with the Ti implant, HA, and HA−CNT coatings and distant bone. Such study enables an indirect prediction of the stress and strains at the implant/bone interface which is critical for the mechanical integrity of the implant. Elastic modulus of Ti, HA coating, and HA−CNT coating before implanting was measured to be 109 $\pm$ 3, 90 $\pm$ 10, and 115 $\pm$ 9 GPa, respectively. These coatings were soaked in formalin for 18 days, and elastic modulus was measured again in the soaked condition to evaluate if there is any effect of formalin soaking on the modulus of coatings. However, the elastic modulus values of the coatings remain similar before and after formalin soaking, indicating the change

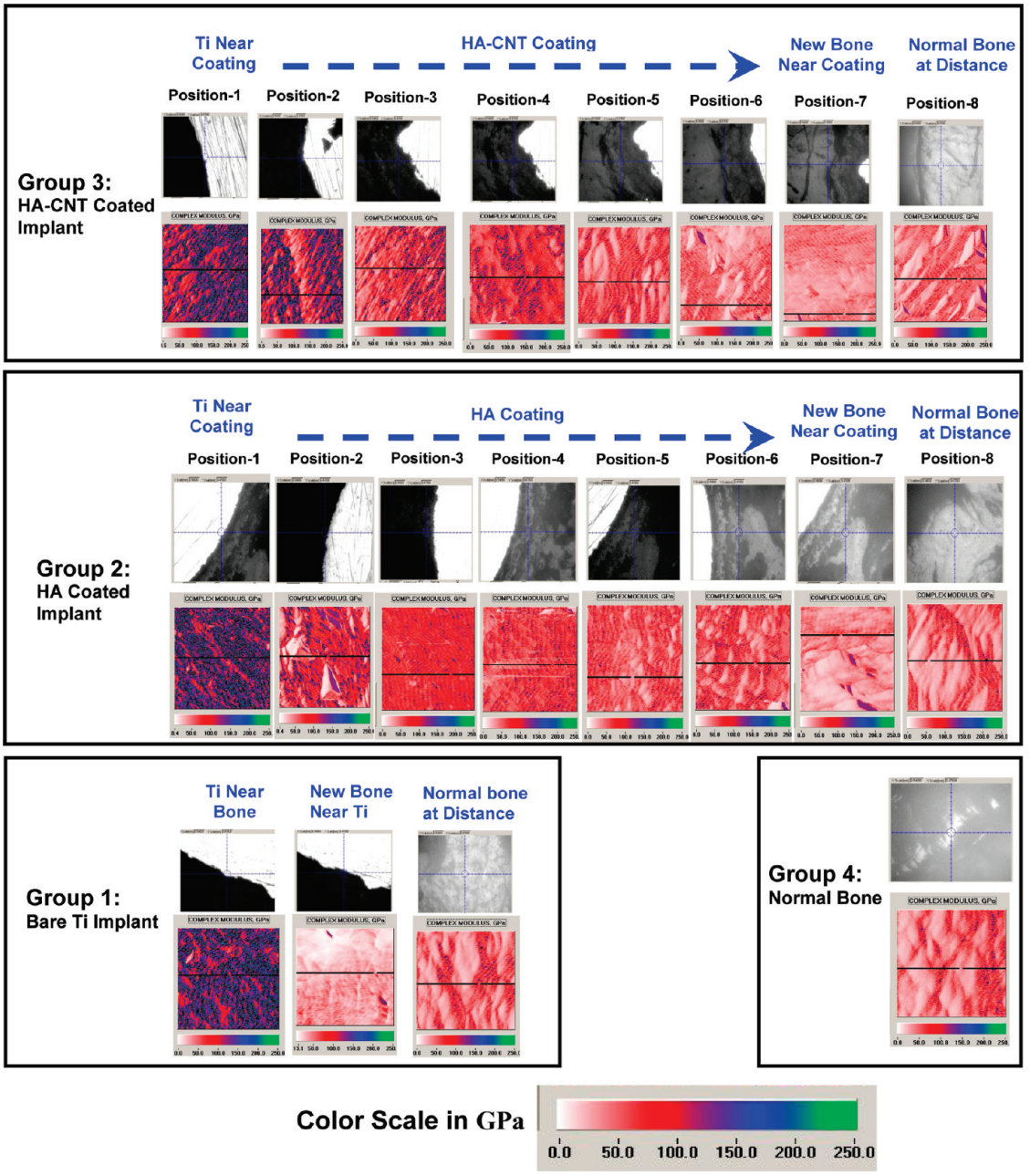

Figure 9. Modulus map from different regions in rat implant/coating/bone interfaces for groups 1−4. Positions of maps in groups 2 and 3 are as shown in Figure 2b. The color scale for modulus maps is similar and varies between 0 and 250 GPa. Titanium in groups 1, 2, and 3 implants shows a high elastic modulus with a dark blue color in the map. Elastic modulus of the coatings (groups 2 and 3) reduces gradually through thickness from near Ti to the bone. The new bone shows the lowest modulus for all groups. Similar modulus for normal bones in all four groups indicates no effect of implant material on the mechanical performance of the normal bone. Group 1 shows a sharp change in the modulus (color) at the implant/bone interface. The change in modulus at the implant/bone interface for groups 2 and 3 is more gradual.

in retrieved implants is due to the *in vivo* exposure only and not due to their preservation in formalin.

Figures 9 and 10 show a decreasing gradient in the elastic modulus of both HA and HA−CNT coatings, which is attributed to the tissue in-growth at the coating/bone interface during new bone formation. During the bone formation process, osteoblasts initially play an active role in the collagen matrix formation on the implant surface. HA-based coatings have porosity in its plasma-sprayed microstructure also due to possible resorption. Due to the porous nature of the coatings, the collagen fibers get impregnated in the coatings,[42] making the integration of bone more effective and at the same time modifying the modulus of the coating. Presence of HA in the coating, which possesses similar chemistry of the mineral content of bone, further helps in bone formation and integration on the coated implant surface.

Figure 10 also shows the effect of CNT addition on the elastic modulus of HA coating. Elastic modulus of

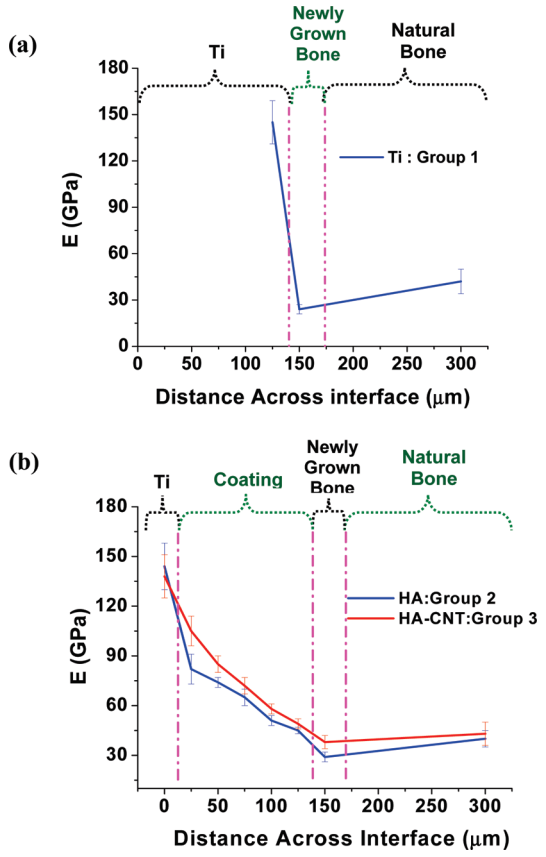

Figure 10. Gradient of elastic modulus across rat bone/implant interface for (a) group 1, Ti implant; (b) group 2, HA-coated Ti implant; and group 3, HA–CNT-coated Ti implant. Elastic modulus values were averaged from the modulus maps presented in Figure 8. Group 1 samples show a sharp change in the elastic modulus at the Ti/bone interface, which pose a risk of fracture or delamination. In groups 2 and 3, the elastic modulus changes gradually through the coating thickness and makes a smoother profile of the modulus at the implant/bone interface with a reduced chance of the failure. The modulus for the Ti part of the implant and normal bone at a distance from the implant remains the same for both groups 2 and 3. CNT reinforcement in HA shows an improvement in the elastic modulus of the HA coating and also the adjacent new bone formed.

the coating remains higher throughout for HA–CNT than for HA, which is clearly due to the reinforcing effect of CNT even after *in vivo* exposure. The newly grown bone near the implant surface shows the lowest modulus in the case of a bare Ti implant (group 1). Presence of HA on the implant surface helps better mineralization of the bone and as a result a higher modulus than the bone near a bare Ti surface. Further, elastic modulus of the bone near the HA–CNT surface shows higher value than the bone at the HA surface. This observation could be explained by the favorable role of CNT in osteoblast proliferation and differentiation reported until now.[9,25] It was found that osteoblasts show better proliferation and viability in the presence of CNTs in the culture surface. Preferential absorption of favorable proteins on the CNT surface is found to be responsible for such behavior.[43] Implanting raw CNTs in a mouse skull is also found to accelere *in vivo* bone growth.[24] In addition, the presence of CNT is reported to inhibit the osteoclast proliferation, which destroys the bone structure.[29] Thus, the presence of CNT also fights out the negative factor of bone growth. As a result, the bone growth near the HA–CNT interface becomes more active, causing higher elastic modulus than the bone near the HA interface, which is a very impressive and attractive finding to be reported for the first time. Elastic modulus for the normal bone in all of the cases, including the bone that was not implanted, shows similar value, indicating no adverse effect of CNT addition on the mechanical health of the bone.

CONCLUSIONS

The major findings of this *in vivo* study suggest that CNTs can be used as nanoreinforcement for the HA composite for orthopedic applications without any negative effect. CNT addition resulted in the growth of new bone and improved osseointegration as observed from the adhesion of HA–CNT coating (group 3). The elastic modulus of the newly grown bone was comparable with the distant bone, suggesting excellent mechanical integrity of the implant. Since it has already been proved in our previous work that plasma-sprayed HA–CNT coatings exhibit improved fracture toughness and wear resistance,[9,10] this *in vivo* study using an animal model bolsters the role of HA–CNT coating for orthopedic implants. It is suggested that longer implantation (one year) is needed to further appreciate the quality of osseointegration and to evaluate safety of HA–CNT coating prior to clinical application. Functionalization of exposed CNTs (Figure 1c) in the HA–CNT composite coating by drugs[23] before implantation could be performed by immersion of coated prostheses in a solution of bone growth factors such as Rh-BMP2 to avoid loosening or treated with antibiotics such as Gentamicine to avoid infection. Hence, this study has potentially far reaching benefits for orthopedic applications. Healing time and osseointegration of biomedical materials for joint replacements could be improved with a HA–CNT composite coating.

MATERIALS AND METHODS

Materials and Processing. The methodology of this study was to implant titanium with and without coatings inside the bone of rodents (mice and rats) and to compare tissue, cell behavior, and bone–interface around the implants using histological and TEM observations. Two geometries of Ti-6Al-4V alloy with and

without coatings were implanted: spherical beads for mice and rods for rats. The spherical beads were 1 mm in diameter, whereas rods were 10 mm long and 2.5 mm in diameter (Figure 1a,b). Spherical titanium beads and rods were coated by a plasma spraying process in tje Plasma Forming Laboratory at Florida International University, Miami, USA. Plasma spraying technique is an FDA-approved process and the most frequently used for depositing HA coatings on orthopedic implants.[1] HA nanorods (length = 100−325 nm, diameter = 25−50 nm, density = 3.2 $g \cdot cm^{-3}$) and multiwalled carbon nanotubes (95% purity, 25−50 nm o.d., length = 0.5−2 μm, density = 2.1 $g \cdot cm^{-3}$) were spray dried together to form an agglomerate which served as the feedstock for plasma spraying.[10] Density of HA and HA−CNT coatings, measured using Archimedes principle and water as immersion medium, is 93.7 and 94.0% TD, respectively. X-ray diffraction patterns from both coatings show HA as the major phase. A small amount of β-TCP phase was also observed which is due to partial dissociation of HA during plasma spraying (Figure S2 in Supporting Information). HA−CNT coating evinced higher fracture toughness of 3 $MPa \cdot m^{1/2}$ as compared to 0.64 $MPa \cdot m^{1/2}$ for HA due to CNT bridging (Figure S3 in Supporting Information).

Surgery. For all *in vivo* studies, animals were acclimated for a minimum of two weeks prior to the experimentation. All procedures were performed with prior received ethical approval and carried out in accordance with the regulations laid down for the animals. The samples were implanted: on male mice (46−54 g, 12 weeks old), a total of 17 ICR (Imprinting Control Region) mice from C. River (Wilmington, MA) were operated; and then on male rats (520−630 g, 17 weeks old), a total of 6 Wistar rats from C. River were operated. The mice and rats were anesthetized with an intraperitoneal injection of ketamine (75 mg/kg) and xylasine (10 mg/kg). The surgical procedure involved removal of the hair over the external part of right lower limb *via* shaving and cleaning. The animals were placed on ventral decubitus, with external rotation and abduction of the lower limb. With strict aseptic conditions, after skin incision, patella and quadricep tendons were released. A circular bone defect on external femoral condyle, 1 mm diameter for mice and 3 mm for rats, was performed using an electrical drill with a sterile round bur under irrigation of sterile normal saline. Through the bony defect, beads for mice and rods for rats were completely introduced inside the distal femoral bone. Patella and quadricep tendons were replaced without sutures, and the skin was closed with nonabsorbable sutures. All animals were examined on a weekly basis for any sign of infection or discomfort on the lower limb for a period of one month. All of the implants were retrieved after one month.

Histology. For histological observations, the bones with the implants were sectioned to a thickness of 1−2 mm, with a low speed diamond saw. Then the samples were fixed in neutral formalin solution of 20%, then decalcified inside acetic acid solution of 10% for 4 days and embedded in paraffin. Ultrathin sections were cut at 70 nm, but then bars on the rats' bones were removed before. Sections were stained with Mallory and hematoxylin-eosin colorations and histologically analyzed by light microscopy. For histological observations of rats' bones, some ultrathin sections were also stained with toluidine blue coloration and histologically analyzed by light microscopy.

Transmission Electron Microscopy. For TEM, samples were fixed in 4% buffered paraformaldehyde solution, decalcified inside acetic acid solution of 10% during 4 days, postfixed with 1% osmium tetroxide in 0.1 M cacodylate buffer for 1 h at 4 °C, dehydrated through graded alcohol, and embedded in Epon 812. Ultrathin sections were cut at 70 μm with a diamond knife and stained with uranyl acetate and lead nitrate and observed with a Morgagni 268 electron microscope.

Nanoindentation. Hysitron Triboindenter TI 900 was used to evaluate elastic modulus (E) of the newly grown bone and HA-based coatings in the retrieved implants evaluated using nanoindentation. The cross sections of the retrieved implant bone (Figure 4a) were cleaned by removing the attached tissues. The elastic modulus across the implant/coating/bone interfaces was determined using "modulus mapping" in nanodynamic analysis (nanoDMA) mode. The tests were carried out on the samples hydrated in formalin.[44] Two-dimensional maps of elastic modulus of the sample surface were produced. In order to prepare the sample surface for nanoindentation experiments, implant cross sections were polished using a wet cloth without any abrasive particles. Abrasive particles were not used to restrict the impregnation of the bone surface with the harder particles, which could influence the mechanical properties. A Berkovich indentation probe of 100 nm radius was used for the measurements. The static and dynamic loads for the measurements were 3 and 1.5 μN, respectively, with an applied frequency of 200 Hz. Each 2D modulus map presented in this study covers a 5 μm × 5 μm area on the sample surface that includes a matrix of equally spaced 256 × 256 points, resulting in 65 536 measurements in each scanning. During the measurement of elastic modulus (E), the bone samples were kept hydrated by adding formalin using a dropper to carry out the tests in wet conditions.

Acknowledgment. A.A. acknowledges the support from the National Science Foundation CAREER Award (NSF-DMI-0547178) and DURIP award from Office of Naval Research (N00014-06-0675). D.L. acknowledges the support from the Dissertation Year Fellowship by University Graduate School, Florida International University. *In vivo* work was supported by the "Alsace contre le Cancer". F.F. thanks the Faculté de Chirurgie Dentaire of Strasbourg for financial support. N.J. is indebted to CHU de Nancy, Hôpital Central, "Chirurgie Orthopédique et Traumatologie" (Contrat d'interface INSERM vers l'hôpital).

Supporting Information Available: TEM observation of retrieved groups 1, 2, and 4 implants, methodology to obtain average elastic modulus from modulus maps, X-ray diffraction patterns of plasma-sprayed HA and HA−CNT coatings, and explanations and picture of the effect of CNT reinforcement on HA. This material is available free of charge *via* the Internet at http://pubs.acs.org.

REFERENCES AND NOTES

1. Campbell, A. A. Bioceramics for Implant Coatings. *Mater. Today* **2003**, *6*, 26–30.
2. Poitout, D. G., Ed. *Biomechanics and Biomaterials in Orthopedics*; Springer: London, 2004; ISBN: 1852334819.
3. Wang, J.; Shaw, L. L. Nanocrystalline Hydroxyapatite with Simultaneous Enhancements in Hardness and Toughness. *Biomaterials* **2009**, *30*, 6565–6572.
4. Iijima, S. Helical Microtubules of Graphitic Carbon. *Nature* **1991**, *354*, 56–58.
5. Hwang, G. L.; Hwang, K. C. Breakage, Fusion, and Healing of Carbon Nanotubes. *Nano Lett.* **2001**, *1*, 435–438.
6. Troiani, H. E.; Miki-Yoshida, M.; Camacho-Bragado, G. A.; Marques, M. A. L.; Rubio, A.; Ascencio, J. A.; Jose-Yacaman, M. Direct Observations of the Mechanical Properties of Single-Walled Carbon Nanotubes and Their Junctions at Atomic Level. *Nano Lett.* **2003**, *3*, 751–755.
7. Muthaswami, L.; Zheng, Y.; Vajtai, R.; Shehkawat, G.; Ajayan, P.; Geer, R. E. Variation of Radial Elasticity in Multiwalled Carbon Nanotubes. *Nano Lett.* **2007**, *7*, 3891–3894.
8. Yu, M. F.; Lourie, O.; Dyer, M. J.; Moloni, K.; Kelly, T. F.; Rouff, R. S. Strength and Breaking Mechanism of Multiwalled Carbon Nanotubes under Tensile Load. *Science* **2000**, *287*, 637–640.
9. Balani, K.; Anderson, R.; Laha, T.; Andara, M.; Tercero, J.; Crumpler, E.; Agarwal, A. Plasma-Sprayed Carbon Nanotube Reinforced Hydroxyapatite Coatings and Their Interaction with Human Osteoblasts *In Vitro*. *Biomaterials* **2007**, *28*, 618–624.
10. Lahiri, D.; Benaduce, A. P.; Rouzaud, F.; Solomon, J.; Keshri, A. K.; Kos, L.; Agarwal, A. Wear Behavior and *In Vitro* Cytotoxicity of Wear Debris Generated from Hydroxyapatite−Carbon Nanotube Composite Coating. *J. Biomed. Mater. A* **2011**, *96*, 1–12.
11. Balani, K.; Chen, Y.; Harimkar, S. P.; Dahotre, N. B.; Agarwal, A. Tribological Behavior of Plasma-Sprayed Carbon Nanotube-Reinforced Hydroxyapatite Coating in Physiological Solution. *Acta Biomater.* **2007**, *3*, 944–951.

12. Lahiri, D.; Singh, V.; Keshri, A. K.; Seal, S.; Agarwal, A. Carbon Nanotube Toughened Hydroxyapatite by Spark Plasma Sintering: Microstructural Evolution and Multiscale Tribological Properties. *Carbon* **2010**, *48*, 3103–3114.
13. Wang, X.; Padture, N. P.; Tanaka, H. Contact-Damage-Resistant Ceramic/Single-Wall Carbon Nanotubes and Ceramic/Graphite Composites. *Nat. Mater.* **2004**, *3*, 539–544.
14. Zhan, G. D.; Kuntz, J. D.; Wan, J.; Muhkerjee, A. K. Single-Wall Carbon Nanotubes as Attractive Toughening Agents in Alumina-Based Nanocomposites. *Nat. Mater.* **2003**, *2*, 38–42.
15. Balani, K.; Agarwal, A. Wetting of Carbon Nanotubes by Aluminium Oxide. *J. Nanotechnol.* **2008**, *19*, 165701–165708.
16. Fioritto, S. *Carbon Nanotubes. Angels or Demons?*, 1st ed.; Pan Stanford Publications: Singapore, 2008; pp 105−133.
17. Cheng, C.; Muller, K. H.; Koziol, K. K. K.; Skepper, J. N.; Midgley, P. A.; Welland, M. E.; Porter, A. E. Toxicity and Imaging of Multi-walled Carbon Nanotubes in Human Macrophage Cells. *Biomaterials* **2009**, *30*, 4152–4160.
18. Kagan, V. E.; Konduru, N. V.; Feng, W.; Allen, B. L.; Conroy, J.; Volkov, Y.; Vlasova, I. I.; Belikova, N. A.; Yanamala, N.; Kapralov, A.; *et al.* Carbon Nanotubes Degraded by Neutrophil Myeloperoxidase Induce Less Pulmonary Inflammation. *Nat. Nanotechnol.* **2010**, *5*, 354–359.
19. Singh, R.; Pantarotto, D.; Lacerda, L.; Pastorin, G.; Klumpp, C.; Prato, M.; Bianco, A.; Kostarelos, K. Tissue Biodistribution and Blood Clearance Rates of Intravenously Administered Carbon Nanotube Radiotracers. *Proc. Natl. Acad. Sci. U.S.A.* **2006**, *103*, 3357–3362.
20. Kostarelos, K. Carbon Nanotubes Fibrillar Pharmacology. *Nat. Mater.* **2010**, *9*, 793–795.
21. Kolosnjaj-Tabi, J.; Hartman, K. B.; Boudjemaa, S.; Ananta, J. S.; Morgant, G.; Szwarc, H.; Wilson, L. J.; Moussa, F. *In Vivo* Behavior of Large Doses of Ultrashort and Full-Length Single-Walled Carbon Nanotubes after Oral and Intraperitoneal Administration to Swiss Mice. *ACS Nano* **2010**, *4*, 1481–1492.
22. Ren, H. X.; Chen, X.; Liu, J. H.; Gu, N.; Huang, X. J. Toxicity of Single-Walled Carbon Nanotube: How We Were Wrong? *Mater Today* **2010**, *13*, 6–8.
23. Kostarelos, K.; Bianco, A.; Prato, M. Promises, Facts and Challenges for Carbon Nanotubes in Imaging and Therapeutics. *Nat. Nanotechnol.* **2009**, *4*, 627–633.
24. Usui, Y.; Aoki, K.; Narita, N.; Murakami, N.; Nakamura, I.; Nakamura, K.; Ishigaki, N.; Yamazaki, H.; Horiuchi, H.; Kato, H.; *et al.* Carbon Nanotubes with High Bone-Tissue Compatibility and Bone-Formation Acceleration Effects. *Small* **2008**, *4*, 240–24.
25. Zanello, L. P.; Zhao, B.; Hu, H.; Haddon, R. C. Bone Cell Proliferation on Carbon Nanotubes. *Nano Lett.* **2006**, *3*, 562–567.
26. Niu, L.; Kua, H.; Chua, D. H. C. Bonelike Apatite Formation Utilizing Carbon Nanotubes as Template. *Langmuir* **2010**, *26*, 4069–4073.
27. Kasai, T.; Matsumura, S.; Iizuka, T.; Shiba, K.; Kanamori, T.; Yadasaka, M.; Iijima, S.; Yokoyama, A. Carbon Nanohorns Accelerate Bone Regeneration in Rat Calvarial Bone Defect. *Nanotechnology* **2011**, *22*, 065102.
28. Hahn, B. D.; Lee, J. M.; Park, D. S.; Choi, J. J.; Ryu, J.; Yoon, W. H.; Lee, B. K.; Shin, D. S.; Kim, H. E. Mechanical and *In Vitro* Biological Performances of Hydroxyapatite−Carbon Nanotube Composite Coatings Deposited on Ti by Aerosol Deposition. *Acta Biomater.* **2009**, *5*, 3205–3214.
29. Narita, N.; Kobayashi, Y.; Nakamura, H.; Maeda, K.; Ishihara, A.; Mizoguchi, T.; Usui, Y.; Aoki, K.; Simizu, M.; Kato, H.; *et al.* Multiwalled Carbon Nanotubes Specifically Inhibit Osteoclast Differentiation and Function. *Nano Lett.* **2009**, *9*, 1406–1413.
30. Sakaguchi, N.; Watari, F.; Yokoyama, A.; Nodasaka, Y. High-Resolution Electron Microscopy of Multi-wall Carbon Nanotubes in the Subcutaneous Tissue of Rats. *J. Electron Microsc.* **2008**, *57*, 156–164.
31. Li, A.; Sun, K.; Dong, W.; Zhao, D. Mechanical Properties, Microstructure and Histocompatibility of MWCNTs/HAp Bio-composites. *Mater. Lett.* **2007**, *61*, 1839–1844.
32. Mears, D. C. Metals in Medicine and Surgery. *Int. Met. Rev.* **1977**, *22*, 119–155.
33. Price, R. L.; Waid, M. C.; Haberstroh, K. M.; Webster, T. J. Selective Bone Cell Adhesion on Formulations Containing Carbon Nanofibers. *Biomaterials* **2003**, *24*, 1877–1887.
34. Akasaka, T.; Watari, F.; Sato, Y.; Tohji, K. Apatite Formation on Carbon Nanotubes. *Mater. Sci. Eng., C* **2006**, *26*, 675–678.
35. Aryal, S.; Bahadur, K. C. R.; Dharmaraj, N.; Kim, K. W.; Kim, H. Y. Synthesis and Characterisation of Hydroxyapatite Using Carbon Nanotubes as a Nanomatrix. *Scripta Mater.* **2006**, *54*, 131–135.
36. Muller, J.; Huaux, F.; Fonseca, A.; Nagy, J. B.; Moreau, N.; Delos, M.; Raymundo-Pinero, E.; Beguin, F.; Kirsch-Volders, M.; Fenoglio, I.; *et al.* Structural Defects Play a Major Role in the Acute Lung Toxicity of Multiwall Carbon Nanotubes: Toxicological Aspects. *Chem. Res. Toxicol.* **2008**, *21*, 1698–1709.
37. Lee, Y.; Geckeler, K. E. Carbon Nanotubes in the Biological Interphase: The Relevance of Noncovalence. *Adv. Mater.* **2010**, *22*, 4076–4083.
38. Cheng, C.; Muller, K. H.; Koziol, K. K. K.; Skepper, J. N.; Midgley, P. A.; Welland, M. E.; Porter, A. E. Toxicity and Imaging of Multi-walled Carbon Nanotubes in Human Macrophage Cells. *Biomaterials* **2009**, *30*, 4152–4160.
39. Kim, J. Y.; Khang, D.; Lee, J. E.; Webster, T. J. Decreased Macrophage Density on Carbon Nanotube Patterns on Polycarbonate Urethane. *J. Biomed. Mater. Res.* **2009**, *88*, 419–426.
40. Konduru, N. V.; Tyurina, Y. Y.; Feng, W.; Basova, L. V.; Belikova, N. A.; Bayir, H.; Clark, K.; Rubin, M.; Stolz, D.; Vallhov, H.; *et al.* Phosphatidylserine Targets Single-Walled Carbon Nanotubes to Professional Phagocytes *In Vitro* and *In Vivo*. *PLoS One* **2009**, *4*, e4398.
41. Cherukuri, P.; Bachilo, S. M.; Litovsky, S. H.; Weisman, R. B. Near-Infrared Fluorescence Microscopy of Single-Walled Carbon Nanotubes in Phagocytic Cells. *J. Am. Chem. Soc.* **2004**, *126*, 15638–15639.
42. Liu, X.; Niebur, G. L. Bone Ingrowth into a Porous Coated Implant Predicted by a Mechano-Regulatory Tissue Differentiation Algorithm. *Biomech. Model. Mechanobiol.* **2008**, *7*, 335–344.
43. Akasaka, T.; Yokoyama, A.; Matsuoka, M.; Hashimoto, T.; Watari, F. Thin Films of Single-Walled Carbon Nanotubes Promote Human Osteoblastic Cells (Saos-2) Proliferation in Low Serum Concentrations. *Mater. Sci. Eng., C* **2010**, *30*, 391–399.
44. Pathak, S.; Swadener, J. G.; Kalidindi, S. R.; Courtland, H. W.; Jepsen, K. J.; Goldman, H. V. J. Measuring the Dynamic Mechanical Response of Hydrated Mouse Bone by Nanoindentation. *Mech. Behav. Biomed. Mater.* **2011**, *4*, 34–43.